

Kinetics and mechanisms of Zn complexation on metal oxides using EXAFS spectroscopy

Darryl R. Roberts,^{a,*} Robert G. Ford,^b and Donald L. Sparks^a

^a Department of Plant and Soil Sciences, University of Delaware, Newark, DE 19717, USA

^b US Environmental Protection Agency, Office of Research and Development, National Risk Management Research Lab, 919 Kerr Research Dr., Ada, OK 74820, USA

Received 17 July 2002; accepted 21 February 2003

Abstract

Zn(II) sorption onto Al and Si oxides was studied as a function of pH (5.1–7.52), sorption density, and ionic strength. This study was carried out to determine the role of the various reaction conditions and sorbent phases in Zn complexation at oxide surfaces. Extended X-ray absorption fine structure (EXAFS) spectroscopy was used to probe the Zn atomic environment at the metal oxide/aqueous interface. For both amorphous silica and high-surface-area gibbsite, Zn sorption kinetics were rapid and reached completion within 24 h. In contrast, Zn sorption on low-surface-area-gibbsite was much slower, taking nearly 800 h for a sorption plateau to be reached. In the case of silica, EXAFS revealed that Zn was in octahedral coordination with first-shell oxygen atoms up to a surface loading of approximately $1 \mu\text{mol m}^{-2}$, changing to tetrahedral coordination as surface loading and pH increased. For the high-surface-area gibbsite system, the Zn–O first-shell distance was intermediate between values for tetrahedral and octahedral coordination over all loading levels. Zn formed inner-sphere adsorption complexes on both silica and high-surface-area gibbsite over all reaction conditions. For Zn sorption on low-surface-area gibbsite, formation of Zn–Al layered double hydroxide (LDH) occurred and was the cause for the observed slow Zn sorption kinetics. The highest pH sample (7.51) in the Zn–amorphous silica system resulted in the formation of an amorphous Zn(OH)₂ precipitate with tetrahedral coordination between Zn and O. Aging the reaction samples did not alter the Zn complex in any of the systems. The results of this study indicate the variability of Zn complexation at surfaces prevalent in soil and aquatic systems and the importance of combining macroscopic observations with methods capable of determining metal complex formation mechanisms.

© 2003 Elsevier Inc. All rights reserved.

Keywords: Zinc sorption; Sorption kinetics; EXAFS; Inner-sphere complexation; Surface precipitation

1. Introduction

The migration of potentially toxic metal ions in soil and sediment environments is often dictated by the complexation of these ions at the interface of solid surfaces and the surrounding solution. In natural environments there exist numerous sorbent phases capable of adsorbing metal ions, namely clay minerals, metal oxides and oxyhydroxides, and organic matter. The sorbent phase may play a significant role in the type, strength, and reversibility of the metal complex formed and, therefore, may dictate to what degree the metal ion is either sequestered or mobilized. In natural, complex matrices such as soils, the most reactive sorbent phases may be the coatings of metal oxides and oxyhydroxides on

clay minerals and organic matter, which occur as the result of weathering of minerals bearing the elements in the oxides (Fe, Al, Mn, and Si) and subsequent reprecipitation [1]. Numerous studies have established the importance of metal oxide surfaces in the retention of metals in adsorption experiments, generally relying on macroscopic observations in an effort to develop accurate complexation models [2–5]. However, metal sorption mechanistic information can only be gleaned using a direct molecular probe [6]. Surface complexation models are further limited since many have been carried out over a limited range of reaction conditions and few have considered precipitation of metal ions as a viable sorption mechanism [7].

One metal ion that has been investigated in many metal sorption studies is zinc (Zn). Zinc is a ubiquitous metal ion in soil and aquatic environments and at background levels it poses no serious threat to biota and vegetation. In areas that

* Corresponding author.

E-mail address: droberts@uottawa.ca (D.R. Roberts).

have elevated levels of Zn as a result of ore smelting, land application of biosolids, or other anthropogenic processes, Zn is often a detriment to the environment [8]. At acidic pH values, Zn toxicity to plants is the third most common after Al and Mn [8]. The degree of Zn bioavailability, and therefore Zn toxicity, is by and large determined by the nature of its complexation to sorbent surfaces in soils. Zn has been shown to form a variety of complexes at the surfaces of clay minerals and metal oxides, often dependent on the reaction conditions under study, including pH, ionic strength (I), reaction time, and Zn surface loading. Huang and Rhoads [9] investigated Zn sorption on several hydrous aluminosilicates over a range of pH, ionic strength, and initial Zn concentrations. They concluded that over most reaction conditions Zn adsorbed on aluminosilicates at constant charge sites and constant potential sites. Only at high pH values did they speculate that $\text{ZnSiO}_{3(s)}$ was forming on aluminosilicate surfaces, but they supplied no direct evidence to support their findings. Chemisorption has been proposed as the primary Zn sorption mechanism to oxide and clay mineral surfaces [10–12]. Others have proposed that Zn may form $\text{Zn(OH)}_{2(s)}$ upon sorption to hydrous Al oxide at pH values above 8, again without providing direct evidence for solid phase formation [5]. The sorption kinetics of Zn on hydroxyapatite showed an initial rapid sorption step followed by a much slower rate of Zn removal from solution. It was conceded that the analytical techniques employed (XRD and SEM) in that study were not sensitive enough to determine if precipitation was a major mechanism at high pH values (>7.0) [13].

Many of the above studies would have benefited by combining macroscopic and kinetic observations with direct spectroscopic tools such as extended X-ray absorption fine structure (EXAFS) spectroscopy. EXAFS is capable of probing a target element in a matrix, providing detailed molecular-scale information on its atomic coordination environment and geometry [14]. EXAFS studies of Zn sorption to various oxides and clay minerals have demonstrated the variability of Zn complexation to a variety of surfaces. Zn reacted with ferrihydrite formed inner-sphere complexes with tetrahedral first-shell oxygen coordination [15], whereas when reacted with goethite Zn formed inner-sphere complexes in a distorted octahedron with oxygen, sharing edges and/or corners with Fe octahedra at the goethite surface [16]. In contrast, Trivedi et al. [17] observed only outer-sphere complexes on hydrous ferric oxide (HFO) and tetrahedral Zn sorption complexes upon reaction with goethite. When reacted with manganite ($\gamma\text{-MnOOH}$), Zn formed a mixture of tetrahedral and octahedral Zn coordination complexes, changing to 100% tetrahedral as pH increased [18]. On both single crystal and powder $\alpha\text{-Al}_2\text{O}_3$, inner-sphere Zn adsorption complexes were in tetrahedral coordination with oxygen, changing to octahedral coordination with the onset of Zn surface precipitation [19,20]. The reason Zn can accept both tetrahedral and octahedral coordination with respect to its first-shell coordination is due to the fact that for each of the two coordination geometries Zn has a value of zero for

its crystal field stabilization energy (CFSE). Moreover, the ionic radius of Zn is intermediate between radius-ratio predictions for the two types of coordination environments [15]. Unlike other transition metals, Zn can switch between the two coordination geometries upon adsorption to mineral and oxide surfaces and is also present in both geometries in minerals such as hydrozincite ($\text{Zn}_5(\text{OH})_6(\text{CO}_3)_2$) [21]. While sorbent phase, reaction pH, surface loading, and other factors have been shown to influence the coordination geometry of Zn sorption complexes, the mechanism of these factors have yet to be gleaned.

In addition to inner- and outer-sphere complex formation, Zn has also been observed to form solid precipitate phases upon reaction with various minerals. Ford and Sparks [22] used EXAFS to observe the formation of a Zn–Al layered double hydroxide (LDH) surface precipitate when reacted with the clay mineral pyrophyllite at pH 7.5. Similarly, Trainor et al. [20] observed Zn precipitate formation on the surface of Zn-reacted $\alpha\text{-Al}_2\text{O}_3$, described as having the structure of a hydroxalite-like phase. In both studies it was suggested that dissolved Al from the sorbent phase was integrated into the precipitate structure [22]. In these studies, and other similar studies with different transition metals (Co and Ni), the neoformed precipitate often formed below pH and metal concentration values that were thermodynamically favorable for known metal hydroxides [24,25]. This suggests that the reduced solubility of these phases may be partially due to the sorbent phase (surface-induced precipitation), but with a lack of solubility data for such phases this remains speculative. Others have observed formation of Zn-bearing phyllosilicates upon reaction of Zn with smectite at near-neutral pH values [23]. Regardless of the sorption mechanism, there is evidence that neoformed solid phases may serve to stabilize metal ions in soil environments, essentially making them less available for plant and microbial uptake or transport into groundwater [26].

In addition to laboratory-based studies, the speciation of Zn in soils and sediments has been shown to vary considerably. Zinc-contaminated soils near metal smelting facilities have been characterized with both bulk and micro-EXAFS to investigate Zn speciation. At circumneutral pH values, Manceau et al. [27] demonstrated that Zn was released from smelter metal-bearing minerals and reprecipitated as a Zn phyllosilicate phase. In a similar investigation on more acidic soils, Roberts et al. [28] observed that after release from smelter-born particles Zn was primarily associated with oxides of Al, Fe, and Mn in both octahedral and tetrahedral coordination with oxygen. Other investigations have observed that upon oxidation of reduced sediments, Zn partially or completely transformed from Zn sulfide to Zn associated with iron oxyhydroxide phases and/or formed Zn-bearing phyllosilicates [29,30]. This type of transformation also occurred seasonally in a contaminated wetland [31].

The EXAFS-based studies that have been reviewed thus far clearly demonstrate the variable reactivity of Zn and the numerous species it can be present as in natural settings.

Understanding the conditions that influence the dynamic behavior of Zn is crucial in order to predict its fate and mobility in these settings. However, with few exceptions, the combination of macroscopic sorption investigations with analytical speciation tools has been neglected. By varying the pH, reaction time, and ionic strength while monitoring Zn sorption mechanisms with EXAFS, one may provide insight into the behavior of Zn sorption and speciation in nature. In order to aid this investigation, two solid phases prevalent in nature and demonstrated to sorb Zn have been selected: gibbsite and amorphous silica. By using two different metal oxides in our study, the degree to which the Zn coordination environment is influenced by the sorbent phase can be determined. Therefore, the objectives of this investigation are to:

- (1) Determine Zn complexation mechanisms on Al and Si oxides as a function of pH, ionic strength, Zn surface loading, and reaction time.
- (2) Assess the influence of the solid phase on the first-shell coordination environment of sorbed Zn.

2. Materials and methods

2.1. Solid materials

The silica used in this study was a Huber Zeofree 5112 amorphous SiO₂ colloid. The point of zero charge (PZC) of amorphous silica was reported to be less than 2 and therefore in this study it was deprotonated over all reaction conditions [9]. The surface area as determined by the BET method was 90 m² g⁻¹ [32]. The gibbsite used in this study was synthesized following the procedure of Kyle et al. [33] to achieve a phase with a high surface area. Briefly, 4 M NaOH was added dropwise to a 1.0 M AlCl₃ solution until a gelatinous precipitate appeared, followed by dialysis for 36 days in DDI (distilled deionized) H₂O. Analysis by X-ray diffraction (XRD) identified the solid as gibbsite, Al(OH)₃, with all Al in octahedral coordination as determined by Al nuclear magnetic resonance (Al NMR). The point of zero salt effect (PZSE) for the gibbsite was at pH 10.1 and its surface area was 96 m² g⁻¹ as determined by the BET N₂ method. This will be referred to as high-surface-area (HSA) gibbsite for the remainder of the paper. A low-surface-area (LSA) gibbsite containing 10% bayerite was obtained from a natural clay deposit (Arkansas, USA, Wards). Its surface area was determined to be 25 m² g⁻¹ with a PZSE at pH 9.0. All solid phases were washed with background electrolyte and hydrated for at least 24 h prior to the onset of Zn(II) sorption experiments.

EXAFS data were collected on Zn-bearing reference minerals to aid in data fitting and for comparison of spectra to sorption samples. These reference minerals included smithsonite (ZnCO₃); hydrozincite (Zn₅(OH)₆(CO₃)₂); zincite (ZnO); synthesized Zn(OH)₂; synthesized Zn–Al layered double hydroxide (Zn–Al LDH); gahnite (ZnAl₂O₄); and

willemite Zn₂SiO₄. With the exception of the synthesized samples, all minerals were donated by the Smithsonian mineral reference library. The Zn–Al LDH phase was synthesized by the method of Taylor [34] in an N₂-purged environment using reagents made with CO₂-free water. Synthetic Zn(OH)₂ was prepared following the procedure of Dietrich and Johnston [35] which showed only amorphous characteristics with X-ray diffraction [15]. Spectra were also collected for a 10 mM aqueous solution of dissolved Zn(NO₃)₂ at pH value 6.02. According to the speciation program MINEQL version 4.1 and the equilibrium constants of Baes and Mesmer [36], Zn²⁺ was the dominant Zn phase in these solutions. The spectrum for hemimorphite was generated from crystallographic data using FEFF 7.0 [37].

2.2. Adsorption experiments

Two different types of sorption experiments were conducted: pH edge experiments (varying pH) and sorption kinetic experiments (varying time). Both experiments used CO₂-free DDI Milli-Q water for preparing solutions. For the pH edges, experiments were carried out in an N₂-purged glovebox. Suspensions of 10 g l⁻¹ (silica or gibbsite) were equilibrated at pH 4 for 24 h in background electrolyte in a 250-ml reaction vessel while constantly stirring using a magnetic stir bar and stir plate. Two separate vessels were used for each sorbent: one for 0.005 M ionic strength and the other for 0.1 M ionic strength, both adjusted using NaNO₃. After this pre-equilibration step, the necessary amount of Zn from an acidified 0.1 M Zn(NO₃)₂ stock solution was added to each vessel in order to achieve an initial Zn concentration of 1 mM. The Zn was added in 100-μl increments over a period of several minutes (waiting at least a minute between aliquot additions) to ensure there was not a local oversaturation of any Zn solid phases in solution. In order to obtain a range of pH values for the pH edge, the pH of the suspensions was incrementally increased by dropwise addition of 0.1 M NaOH. Following each rise of approximately 0.4 pH units, a subsample of the suspension was removed with a pipette and transferred to a 40 ml centrifuge tube. Next, each tube was placed on an end-over-end shaker in the glovebox and allowed to react for 24 h. Enough subsamples were transferred so that a pH range from 4.5 to 8.5 was obtained. The experimental pH was taken to be the pH measured after a 24 h reaction time. After 24 h, the solids were separated from the suspensions by centrifugation at 12,000 rpm for 15 min. The supernatants were passed through 0.2-μm cellulose filters, acidified, and analyzed for Zn using atomic absorption spectrometry (AAS). The amount of Zn sorbed was calculated to be the initial Zn concentration minus the Zn concentration in solution.

For the Zn sorption kinetic studies, experiments were carried out using a pH-stat apparatus equipped with a delivery burette filled with CO₂-free 0.1 M NaOH. The kinetic experiments were performed outside the glovebox using CO₂-free DDI Milli-Q water to prepare all solutions. During the ex-

periments N_2 was rapidly bubbled through the suspension to minimize the amount of $CO_{2(g)}$ entering the system. The reaction vessel was covered with a Plexiglass lid and Parafilm was used to seal any leaks which might have allowed $CO_{2(g)}$ penetration into the system. Sorption kinetics were carried out at $pH\ 7.5 \pm 0.05$ with $[Zn]_0 = 1\ mM$ and $I = 0.1\ M$ in $NaNO_3$. All suspension densities were $10\ g\ l^{-1}$. After pre-equilibrating the solid phases in each of the appropriate background electrolyte solutions for at least 24 h, Zn from a $0.1\ M\ Zn(NO_3)_2$ stock solution was added to the reaction vessels in $100\text{-}\mu\text{l}$ increments over a period of at least 10 min. The experimental conditions were selected for comparison to numerous studies that have identified metal hydroxide formation at or near $pH\ 7.5$ for metal sorption to clay minerals and oxides [20,22,36,38,39]. After the proper reaction time, samples were removed from the vessel and centrifuged at 12,000 rpm for 15 min followed by filtration, acidification, and analysis for Zn using AAS. The amount of Zn sorbed was taken to be the difference between the amount remaining in solution and the initial Zn concentration.

2.3. EXAFS sample preparation and spectral analysis

EXAFS samples were prepared in the same manner as the sorption edges were, with a sample size large enough to yield at least 50 mg of solid for analysis. The solid suspension density, $[Zn]_0$, ionic strength, and pH were varied to determine the effects of these reaction conditions on Zn speciation (Table 1). One sample each from the Zn–gibbsite and Zn–silica systems were aged 18 months in a temperature-controlled incubation chamber while being gently agitated on an orbital shaker. The pH values for these aged samples were checked and adjusted weekly. For the low-loading samples ($\Gamma < 0.5\ \mu\text{mol}/\text{m}^2$) centrifugation and decantation

would have resulted in a significant amount of Zn in solution, potentially resulting in a signal from aqueous Zn^{2+} . To minimize these signals, a complete separation of the solid paste from solution via vacuum filtration through a $0.2\text{-}\mu\text{m}$ cellulose filter was employed in lieu of centrifugation and decantation. This eliminated the need to wash the sample and potentially desorb any Zn from the sample. By determining the amount of Zn remaining in interstitial electrolyte using a mass balance, it was estimated that the aqueous Zn^{2+} did not significantly contribute to the overall EXAFS signal [40,41].

Zn *K*-edge EXAFS spectra were recorded at Beamline X-11a at the National Synchrotron Light Source (NSLS), Brookhaven National Laboratory, Upton, NY. The beam current at NSLS varied from 100 to 300 mA at 2.5 GeV. The beamline monochromator consisted of two parallel Si(111) crystals adjusted to an entrance slit of 1 mm. Higher order harmonics were suppressed by reducing I_0 (incoming energy) by 25% after optimization of the incoming beam. The beam energy was calibrated by assigning the first inflection to the absorption edge of metallic Zn foil to an energy value of 9659 eV. For sorption samples, slightly moist pastes were mounted in aluminum sample holders and sealed with Kapton tape. For reference samples, dry powders were diluted to 10% in a boron nitride powder to prevent the detector from being swamped. Samples were scanned in fluorescence mode at $25\ ^\circ\text{C}$ using an Ar-filled Stern–Heald type (Lytle) detector equipped with a $3\text{-}\mu\text{m}$ Cu filter [42]. At least three scans were collected per sample to increase the signal to noise ratio.

Numerical results were extracted from the EXAFS spectra using WinXAS version 1.3 [43] combined with the FEFF 7.0 code [44]. The background was subtracted using a linear fit through the pre-edge region and a second order

Table 1
Sample preparation conditions for Zn(II) sorption on metal oxides

Sample ^a	Sorbent	Final pH	Reaction time	Initial Zn conc.	Solid/solution ratio	Ionic strength (M) ^b	Γ ($\mu\text{mol}/\text{m}^2$) ^c
A		6.02		10 mM	$Zn(NO_3)_2(\text{eq})$		
B	SiO ₂	5.10	24 h	1 mM	5 g/l	0.0048	0.07
C	SiO ₂	6.12	24 h	1 mM	5 g/l	0.049	0.3
D	SiO ₂	6.56	24 h	1 mM	5 g/l	0.11	1.06
E	SiO ₂	7.45	24 h	0.1 mM	3 g/l	0.10	0.35
F	SiO ₂	7.35	24 h	1 mM	10 g/l	0.12	1.01
G	SiO ₂	7.35	18 months	1 mM	10 g/l	0.11	1.04
H	SiO ₂	6.83	24 h	2 mM	5 g/l	0.10	2.92
I	SiO ₂	7.51	24 h	1 mM	5 g/l	0.11	2.08
J	Al(OH) ₃	6.03	24 h	1 mM	5 g/l	0.005	0.31
K	Al(OH) ₃	6.56	24 h	1 mM	10 g/l	0.10	0.68
L	Al(OH) ₃	7.50	24 h	0.1 mM	3 g/l	0.11	0.36
M	Al(OH) ₃	7.50	24 h	1 mM	10 g/l	0.10	1.79
N	Al(OH) ₃	7.52	18 months	1 mM	10 g/l	0.10	1.04
O	Al(OH) ₃	7.10	24 h	2 mM	5 g/l	0.12	2.89
P	Al(OH) ₂ ^d	7.47	24 h	1 mM	10 g/l	0.11	3.76

^a Sample letters correspond to spectra in Figs. 4(A–I) and 5(J–P).

^b Ionic strength adjusted using $NaNO_3$.

^c Zn surface coverage.

^d Low-surface-area gibbsite.

polynomial beyond the edge. The chi function was extracted from the background-subtracted raw data by fitting a linear function to the pre-edge region and a six-knot spline function to the post-edge region. The data were converted to k space by applying the EXAFS equation and subsequently weighted by k^3 to compensate for damping of oscillations at high k . The k^3 data were fit over similar k -ranges ($k \approx 1.5$ to 12) using a nonlinear least-squares approach with theoretical values for Zn–O, Zn–Si, Zn–Zn, Zn–Al, and Zn–C bonds from FEFF 7.0 using structural refinement data for ZnO, ZnSi₂O₄, Zn–Al layered double hydroxide, and ZnCO₃. Spectra were also Fourier transformed (Bessel window) to produce radial structure functions (RSFs) that isolate frequency correlations between the central absorbing atom (Zn) and neighboring atoms as a function of bond distance (R). In addition to k -space fits, R -space fits were performed by isolating the first and second (when present) coordination shells. The amplitude reduction factor was set to 0.90, a value obtained by setting the coordination number (CN) for Zn in known octahedral coordination (Zn(NO₃)₂) to 6 and using the obtained value. The same value has been used by researchers studying similar systems [22]. The errors in the first and second shell bond distances (R) were estimated to be accurate to ± 0.02 Å and CN were accurate to $\pm 30\%$. The errors were estimated by comparison of XRD structural refinement data of known reference minerals to fit parameters estimated by collecting EXAFS on the same minerals and applying nonlinear least-squares analysis of the spectra [29,45].

3. Results and discussion

3.1. Macroscopic Zn sorption

The effects of ionic strength and pH on Zn adsorption on silica and gibbsite are shown in Fig. 1. For both the gibbsite and silica systems, a rapid increase from nearly 0% to nearly 100% Zn removal (within detection limit of the AAS) occurred over a very small pH range, commonly known as a pH edge. The pH edge for Zn on gibbsite was shifted to the left relative to the Zn on silica, with approximately 50% of Zn removed at pH 6.6 for Zn–gibbsite and at pH 6.9 for Zn–silica (based on inflection points). In both cases the adsorption was ionic-strength-independent, suggesting an inner-sphere Zn complex to the surface of these solids as metal sorption via this mechanism can occur regardless of the solid surface charge [46]. At pH 7.5 the silanol groups on the amorphous silica were most likely entirely deprotonated ($pK_a < 2$), while the aluminol groups on gibbsite may be partially deprotonated ($pK_a = 10$). Numerous metal sorption studies have revealed similar pH edges and they were typically attributed to adsorption at pH-dependent surface sites [9,47]. This type of sorption behavior would result in proton release from the solid as the metal binds to the surface, with the exact amount depending on the sorption complex formed [3].

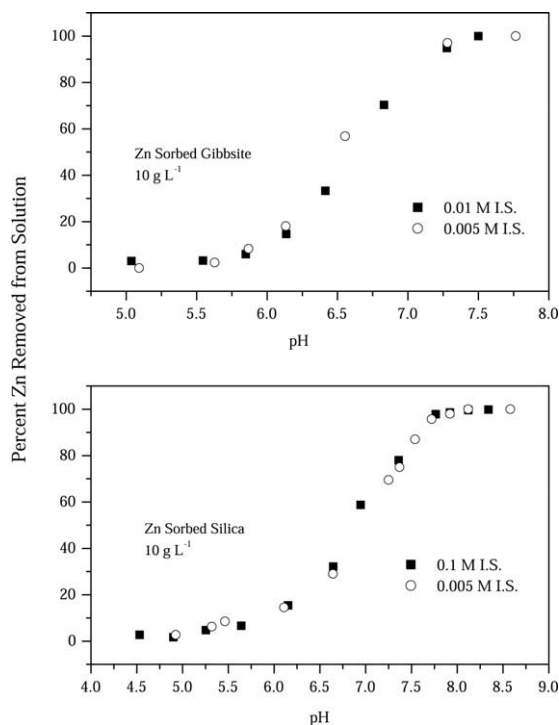


Fig. 1. Zn sorption (pH) edges on low and high surface area gibbsite (top panel) and on silica (bottom panel) at I.S. = 0.1 M and I.S. = 0.005 M NaNO₃.

In all experiments, constant base addition was required to maintain a nearly constant pH value suggesting Zn sorption at pH-dependent sites. However, macroscopic observations of Zn sorption alone cannot determine exact modes of uptake as the adsorption of metals from solution is not necessarily a singular process and there may be a continuum between outer-sphere complexation, inner-sphere complexation, and surface precipitation [46].

Figure 2 illustrates the kinetics of Zn sorption on LSA and HSA gibbsite (top panel) and on amorphous silica (bottom panel). Both systems had the same reaction conditions (1 mM [Zn]₀ and pH 7.5). For both Zn–silica and Zn–HSA gibbsite, Zn was removed from solution quite rapidly, with both systems eventually removing nearly all of Zn from solution. For the Zn–silica system, Zn removal was extremely rapid with over 80% of added Zn removed from solution by the time the first sample was collected (15 min). Thereafter the sorption kinetics slowed slightly and 100% removal was achieved within 3 h. For the Zn–HSA gibbsite system, slightly slower sorption kinetics was demonstrated relative to the Zn–silica system. For Zn on HSA gibbsite, 80% of Zn was removed from solution after 24 h and a slightly slower second sorption step followed, with nearly complete Zn uptake within 200 h. The slight contrast in Zn sorption kinetics between the silica and HSA gibbsite systems is noteworthy since both solids have similar surface areas (90 m² g⁻¹ for silica and 96 m² g⁻¹ for HSA gibbsite). This suggests that total surface area was not the sole factor controlling Zn sorption kinetics, but the reactivity of the specific surface sites on

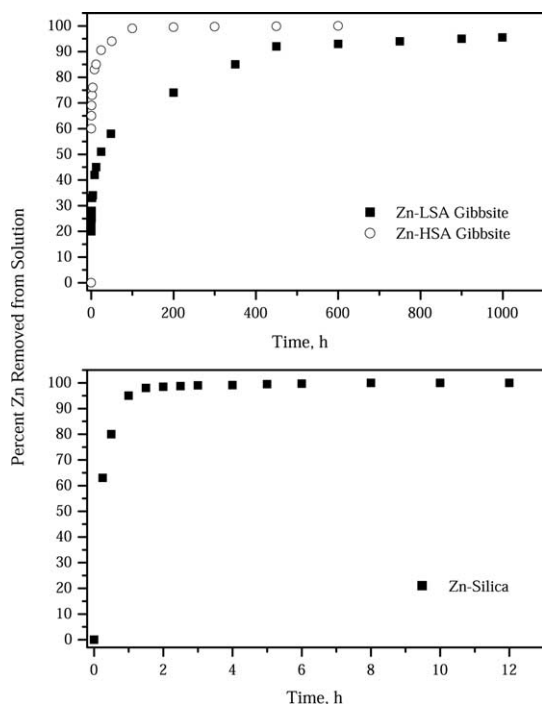


Fig. 2. Zn sorption kinetics on low-surface-area gibbsite and high-surface-area gibbsite (top panel) and amorphous silica (bottom panel).

the two solids is also important. As previously noted, silica has more negatively charged sites under the reaction conditions studied.

The effect of surface area on the kinetics of Zn sorption is evident in comparing the LSA and HSA gibbsite systems (Fig. 2, top panel). Like the Zn–HSA gibbsite system, Zn

sorption onto LSA gibbsite demonstrated a rapid initial sorption step followed by a much slower sorption step. In contrast to the HSA gibbsite system, only 50% of the Zn sorption was complete within the first 24 h in the LSA gibbsite system and the second, slower sorption step had a more linear shape. The same observations were made for Ni sorption on HSA and LSA gibbsite by Yamaguchi et al. [48]. They attributed the difference to chemisorption playing the dominant role in Ni removal on HSA gibbsite, whereas surface-induced precipitation of α -Ni(OH) $_{2(s)}$ controlled the kinetics of Ni removal in the LSA system. Other investigators have observed slow metal sorption onto gibbsite [38,49]. To verify the mechanisms responsible for the differences between these two gibbsite systems and for identification of Zn surface complexes on all metal oxides, EXAFS studies were performed.

3.2. EXAFS analysis of Zn reference compounds

The k^3 -weighted Zn EXAFS spectra (χ) and their corresponding Fourier-transformed radial structures (RSFs) for reference Zn minerals and aqueous Zn $^{2+}$ are presented in Fig. 3. R -space (right panel) fits from nonlinear, least-squares analysis are represented by the dashed lines while the solid lines represent the raw data. The results from the fits along with comparison to XRD data for the same reference phases are presented in Table 2. The spectra in Fig. 3 demonstrate the kinds of features one would expect in EXAFS data if neoprecipitated phases form relative to samples where adsorption is the primary mechanism of Zn removal from solution. The Zn reference minerals have second-neighbor Zn,

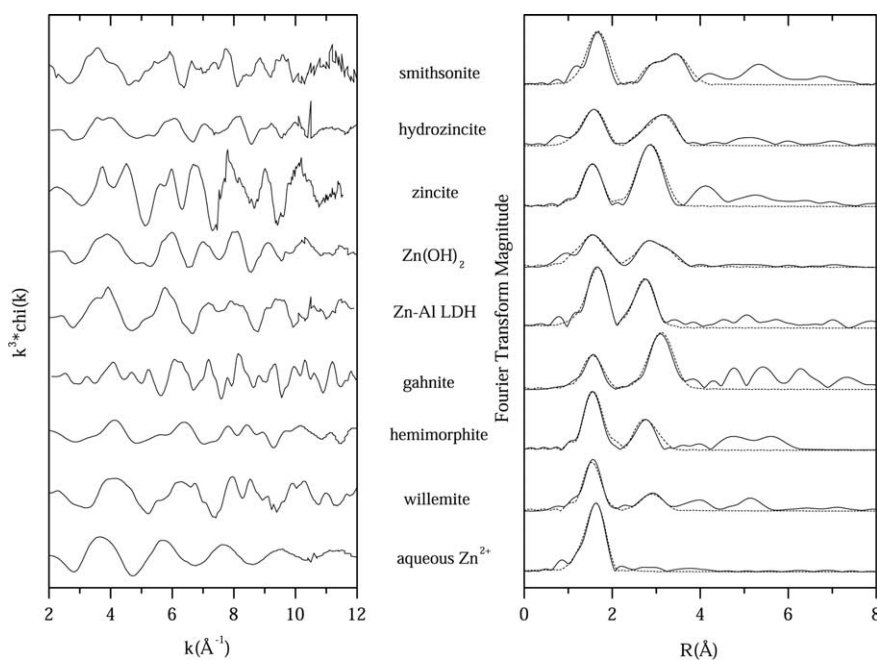


Fig. 3. Zn–EXAFS χ spectra weighted by k^3 (left panel) and corresponding Fourier transforms for Zn-bearing reference compounds. The results from the nonlinear least-squares fit are the dashed lines in the right panel. The spectrum for hemimorphite was generated from FEFF 7.0 using XRD structural refinement data.

Table 2
Local structures of Zn model compounds derived from EXAFS and XRD

Compound	Formula	Atom	EXAFS ^a <i>R</i> (Å) ^c	XRD		Reference ^b
				CN ^d	<i>R</i> (Å)	
Smithsonite	ZnCO ₃	Zn–O	2.10	6	2.11	[60]
		Zn–Zn	3.71	6	3.67	
		Zn–C	3.34	2.2	3.29, 3.50	
Hydrozincite	Zn ₃ (OH) ₆ (CO ₃) ₂	Zn–O	2.02	4.6	1.95, 2.10	[21]
		Zn–Zn	3.22	2.6	3.15, 3.57	
Zincite	ZnO	Zn–O	1.95	4	1.98	[61]
		Zn–Zn	3.22	12	3.50, 3.66	
Zinc hydroxide	Zn(OH) ₂	Zn–O	1.99	4	1.96	[62]
		Zn–Zn	3.29, 3.47	2.2	3.29, 3.50	
ZnAl layered double hydroxide (LDH) ^e	(Zn _x Al _{1-x}) (OH) ₂ (NO ₃) ₂ H ₂ O	Zn–O	2.07	6.6	2.01, 2.04	[63]
		Zn–Al	3.06	6	3.05–3.08	
		Zn–Zn	3.1	6	3.05–3.08	
Gahnite	ZnAl ₂ O ₄	Zn–O	1.97	4	1.93	[64]
		Zn–Al	3.41	12	3.35	
		Zn–Zn	3.55	4	3.50	
Hemimorphite ^f	Zn ₄ Si ₂ O ₇ (OH) ₃ H ₃ O	Zn–O		4	1.94–1.97	[65]
		Zn–Zn	3.33	4.4	3.28, 3.46	
Willemite	Zn ₄ SiO ₄	Zn–O	1.95	4	1.97	[66]
		Zn–Zn	3.25	2	3.23	
Aqueous Zn ²⁺	Zn(H ₂ O) ₆	Zn–O	2.07			N/A

^a EXAFS parameters derived from single shell fitting for Zn–O, Zn–C, Zn–Al, and Zn–Zn, so distances represent the average value.

^b Reference refers to XRD structural refinement data.

^c Interatomic distance.

^d Coordination number.

^e Based on substitution of Zn for Mg in a hydrotalcite structure.

^f The hemimorphite EXAFS structure generated from crystallographic data using FEFF7.

Si, C, and Al atoms present around the central Zn atom, resulting in the significant amount of structural features in the chi spectra. Upon Fourier transforming the data, one notes the presence of peaks beyond the first-shell Zn–O peak that can be attributed to the presence of the second neighbor atoms in some combination, depending on the precipitate phase and Zn coordination environment. Moreover, additional peaks beyond the first- and second-shell peaks are observed in most RSF spectra due to multiple scattering paths.

3.3. EXAFS analysis of Zn-reacted silica

The k^3 -weighted Zn spectra and their results from non-linear least-squares fitting (dashed lines) for Zn reacted with silica are presented in the left panel of Fig. 4. The Fourier transforms of the chi spectra and their fits are presented in the right panel. Each of the chi spectra is characterized by a sine wave dominated by backscattering from first-shell oxygen atoms around the central Zn atom, with the signal amplitude decreasing as k increases. The radial structure functions clearly demonstrate this characteristic Zn–O contribution indicated by large peaks at approximately 1.92 and 2.05 Å. The radial structure functions are uncorrected for phase shift so the value on the x -axis does not necessarily indicate the true bond distance, R . In addition to the first-shell Zn–O, a smaller second shell is evident in the RSF spectra for all samples. The lack of significant structural features and

diminishment of the signal at higher k values in the chi spectra indicate no heavy backscattering atoms, such as Zn, are present around the central Zn atom. This is in contrast to the chi spectra for those samples in which a heavy second neighbor backscattering atom is present (Fig. 3). However, in chi spectra E–I, the second oscillation is less symmetric than in spectra B–D, suggesting a shoulder is forming on the high k side of this oscillation. Given the samples with this feature also have higher surface loading and pH values, it follows that there may be a slight scattering from a second shell Zn atom. However, only spectrum I was able to have a Zn atom fit in its second shell.

Chi spectra E–I are shifted to slightly higher k values relative to spectra B–D (see dotted lines as a guide). This shift to higher k values is indicative of a lower CN_{Zn–O}, namely tetrahedral Zn–O coordination versus octahedral Zn–O first-shell coordination. This shift in the spectra as a function of Zn coordination is also evident for the reference minerals. Comparing tetrahedral Zn–O compounds willemite and hemimorphite to octahedral aqueous Zn²⁺ and smithsonite, a shift to higher k values is observed by an amount consistent with the shift in the Zn–silica system (Fig. 3). As previously noted, Zn has commonly been found in both four- and sixfold coordination environments with first-neighbor oxygen atoms in many aqueous compounds and solid phases [17,20]. The characteristic Zn–O distance in tetrahedral coordination has been reported to be between 1.92 and 1.99 Å,

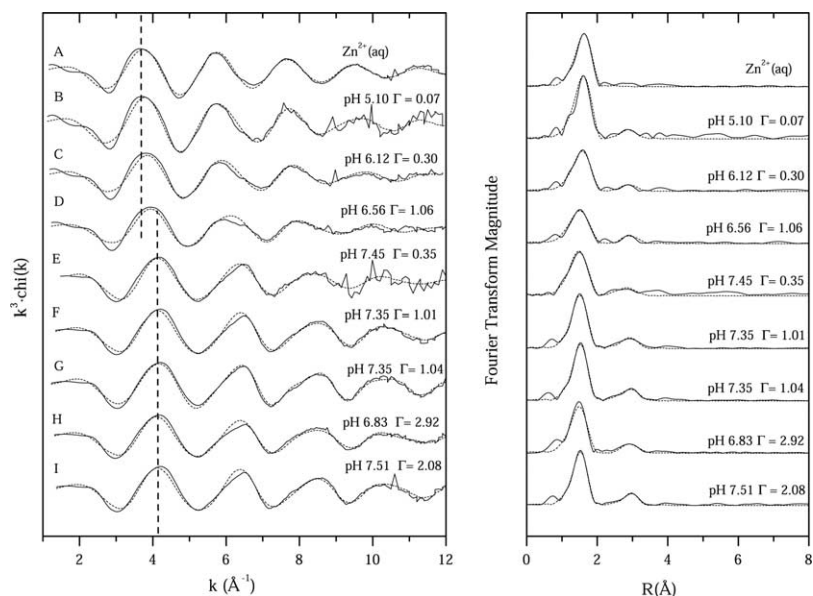


Fig. 4. Zn-EXAFS chi spectra (left panel) weighted by k^3 (solid lines) and results from nonlinear least-squares fitting (dashed lines) for Zn sorbed on amorphous silica (B–I). Corresponding Fourier transforms and R -space fit results (dashed lines) are in the right panel. The vertical lines in the left panel serve as a guide to distinguish between octahedral Zn (shifted left) and tetrahedral Zn (shifted right).

Table 3
Structural parameters from EXAFS analyses of Zn sorbed onto silica

Sample	Zn–O			Zn–Si			Zn–Zn		
	R (Å) ^a	CN ^b	σ^2 ^c	R (Å)	CN	σ^2	R (Å)	CN	σ^2
(A) Aqueous Zn ²⁺	2.07	5.5	0.0080						
(B) pH 5.10, $\Gamma^d = 0.07$	2.05	6.9	0.0062	3.07	0.7	0.0089			
(C) pH 6.12, $\Gamma = 0.30$	2.02	5.3	0.0034	3.06	0.8	0.0092			
(D) pH 6.56, $\Gamma = 1.06$	1.98	4.4	0.0052	3.08	1.0	0.0087			
(E) pH 7.45, $\Gamma = 0.35$	1.93	4.9	0.0034	3.10	1.0	0.0078			
(F) pH 7.35, $\Gamma = 1.01$	1.92	5.2	0.0026	3.11	1.2	0.0063			
(G) pH 7.35, $\Gamma = 1.04$	1.92	4.2	0.0037	3.11	1.4	0.0094			
(H) pH 6.83, $\Gamma = 2.92$	1.92	4.5	0.0046	3.10	1.1	0.0087			
(I) pH 7.51, $\Gamma = 2.08$	1.92	5.3	0.0054	3.13	1.3	0.0076	3.29	1.5	0.0090

^a Interatomic distance.

^b Coordination number.

^c Debye–Waller factor.

^d Zn surface coverage, $\mu\text{mol}/\text{m}^2$.

while Zn in octahedral coordination with first-shell O has a Zn–O distance between 2.02 and 2.12 Å [50]. Given the greater error associated with the CN value compared to the value of R , we use R to classify sorption complexes as either tetrahedral, octahedral, or some combination of both.

The fit results for Zn sorbed on silica are presented in Table 3. Results indicate that Zn is in octahedral coordination with first-shell O atoms in aqueous Zn²⁺ as indicated by $R_{\text{Zn–O}} = 2.07$ Å. For the lowest Zn loading levels of $\Gamma = 0.07$ and $0.30 \mu\text{mol}/\text{m}^2$ at pH 5.10 and 6.12, respectively, the $R_{\text{Zn–O}}$ values are indicative of Zn in octahedral coordination with first-shell O atoms. The small second-shell feature is also observed in these two spectra and could be fit with <1 Si atoms at distances of 3.07 and 3.06 Å, respectively. At higher pH values, the values for $R_{\text{Zn–O}}$ and $\text{CN}_{\text{Zn–O}}$ decreased, indicating the transition from octahedral

Zn–O to tetrahedral Zn–O. This is visually observed in the chi spectra (Fig. 4) as a shift in the entire spectrum from low k to higher k . Excluding sample D at pH 6.56, the average $R_{\text{Zn–O}} = 1.92$ Å and average $\text{CN}_{\text{Zn–O}} = 4.8$. Although sample D has a higher surface loading value compared to sample E it has a larger $R_{\text{Zn–O}}$ and $\text{CN}_{\text{Zn–O}}$, suggesting that pH plays a more significant role than surface loading value alone. For spectra E–H the average $R_{\text{Zn–Si}} = 3.11$ Å and $\text{CN}_{\text{Zn–Si}} = 1.2$. The measured bond distances are indicative of bonding between Zn tetrahedra and Si tetrahedra in a monodentate manner, based on average O–O edge distances ranging from 2.58 to 2.67 Å in SiO₄ tetrahedra [20, 51]. For the two low-loading samples, the shorter Zn–Si distance suggests a bidentate inner-sphere complex, however, this observation is only based on the fact that bidentate complexes typically have shorter metal–metal distances relative

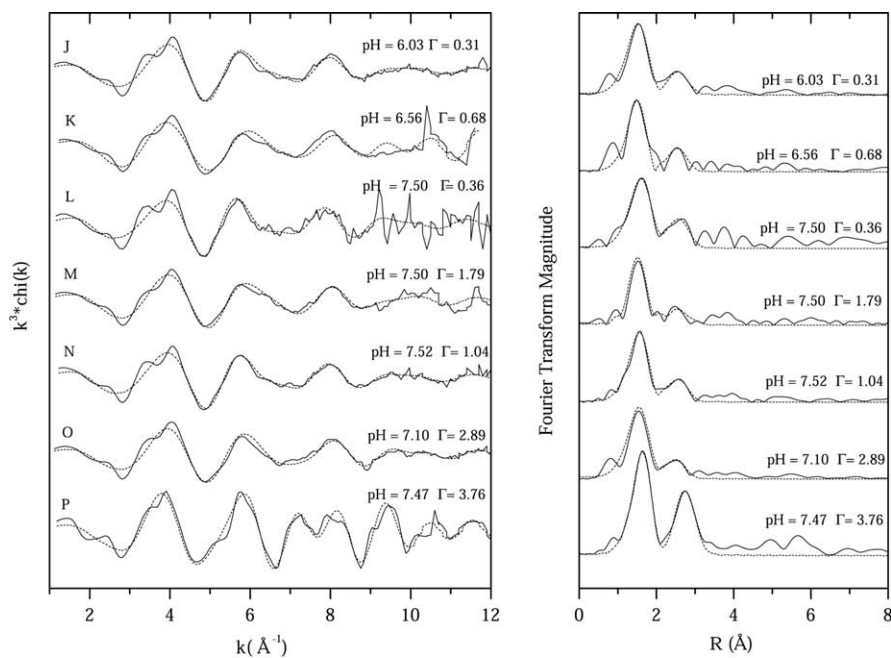


Fig. 5. Zn-EXAFS chi spectra weighted by k^3 (solid lines) and results from nonlinear least-squares fitting (dashed lines) for Zn sorbed on high-surface-area gibbsite (J–O) and low-surface-area gibbsite (P). Corresponding Fourier transforms and R -space fit results (dashed lines) are in the right panel.

to monodentate complexes [51]. The only sample that improved in fit quality by including a second neighbor Zn atom was spectrum I (Table 3), reacted at pH 7.51 with $\Gamma = 2.08 \mu\text{mol m}^{-2}$. The $R_{\text{Zn-Zn}}$ value for this sample was 3.29 \AA and $N_{\text{Zn-Zn}}$ was 1.5. Although this sample has a lower surface loading relative to sample H, the pH value of the reaction was 0.7 units greater, suggesting a minimum pH value needed to be reached prior to the onset of precipitation of a Zn-bearing phase. The $R_{\text{Zn-Zn}}$ of 3.29 \AA is nearest the value of 3.29 \AA for $R_{\text{Zn-Zn}}$ in synthesized amorphous $\text{Zn}(\text{OH})_2$, and both Zn–O shells are in fourfold coordination (Table 3). The sample aged for 18 months (spectrum G, Table 3) at pH 7.2 had no effect on the overall Zn speciation, with Zn remaining as an inner-sphere monodentate complex to silica tetrahedra without the onset of precipitation. Again, this suggested that only at pH 7.51 does a precipitate phase begin to form.

3.4. EXAFS analysis of Zn-reacted gibbsite

The k^3 -weighted Zn EXAFS spectra (chi) and their corresponding RSFs are presented in Fig. 5 (raw data = solid lines, fit data = dashed lines). Much like the EXAFS spectra for the Zn–silica samples (Fig. 4), each of the chi spectra is characterized by a sine wave dominated by backscattering from first-shell oxygen atoms around the central Zn atom with the signal amplitude decreasing as k increases. In contrast to the Zn–silica samples, the chi spectra have more structural features relative to the spectra for aqueous Zn^{2+} . The most striking difference between the Zn–silica and Zn–gibbsite spectra is the split in the first oscillation of the chi spectra at $k \approx 4 \text{ \AA}^{-1}$ for the Zn–gibbsite samples (spec-

tra J–O). The k -space fits (dotted lines) failed to accurately reproduce this feature, suggesting that the fitting approach is insensitive to such a feature or the origin of the split is due to features beyond the second shell around the central Zn atom. Manceau [52] observed a similar feature in the Zn EXAFS of lithiophorite, a mineral composed of interlayered MnO_2 and $\text{Al}(\text{OH})_3$ sheets with Zn substituting into the gibbsitic layer. The splitting in this case was attributed to Al atoms in the second coordination sphere of Zn and was absent in samples in which Zn was associated with heavier second-neighbor atoms such as Fe [53]. Similar EXAFS spectral features were observed in soils in which Zn was directly bound to Al minerals [28,53]. Since including an Al atom in the k -space fits did not properly fit the data at low k values, Fourier back transformations of the RSF spectra were performed to determine the reason for this splitting feature in our samples.

Figure 6 displays Fourier back transformations of the RSF data performed for a representative Zn–gibbsite sample (spectra J, Fig. 5) and a Zn–silica sample (spectra H, Fig. 4). Both spectra display comparable spectral noise in the chi data. The back transformations were carried out over different values in R space (indicated by the shaded regions in the left hand panel of Fig. 6) in order to determine the portion of the spectra responsible for the splitting feature at low k . As the Zn–gibbsite RSF spectrum is back-transformed over values beyond 5 \AA , one notes the presence of the low- k splitting feature near 2 \AA^{-1} in the right panel. This clearly demonstrates the split is due to the RSF backscatter peaks beyond 5 \AA : multiscattering contributions due to atoms beyond the second coordination sphere of the central Zn atom.

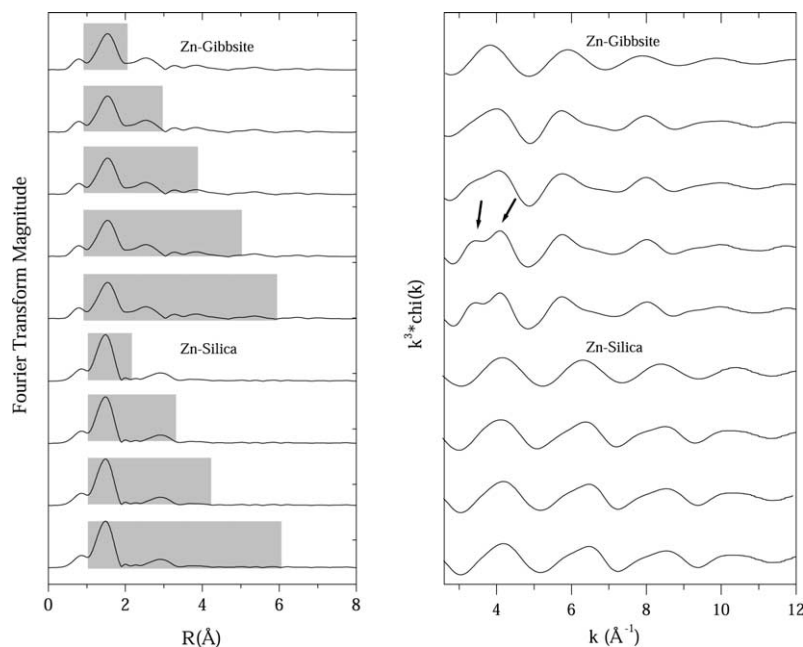


Fig. 6. Fourier transformed EXAFS data for Zn–HSA gibbsite and Zn–amorphous silica samples (left panel) and corresponding Fourier back-transformed spectra (right panel) taken over various ranges of R (Å) as indicated by the shaded regions. The Zn–gibbsite spectra (top 5) are all the same sample (spectra J, Fig. 5) as are the Zn–silica spectra (bottom 4; spectra H, Fig. 4).

Table 4
Structural parameters from EXAFS analyses of Zn sorbed to aluminum oxides

Sample	Zn–O			Zn–Al			Zn–Zn		
	R (Å) ^a	CN ^b	σ^2 ^c	R (Å)	CN	σ^2	R (Å)	CN	σ^2
(J) pH 6.03, $\Gamma^d = 0.31$	2.01	5.1	0.0071	3.02	4.3	0.0100			
(K) pH 6.56, $\Gamma = 0.68$	2.00	4.7	0.0058	3.00	1.9	0.0061			
(L) pH 7.50, $\Gamma = 0.36$	2.06	6.1	0.0062	3.05	3.9	0.0082			
(M) pH 7.50, $\Gamma = 1.79$	2.02	4.9	0.0006	3.02	1.6	0.0072			
(N) pH 7.52, $\Gamma = 1.04$	2.01	4.6	0.0043	3.01	2.6	0.0068			
(O) pH 7.10, $\Gamma = 2.89$	2.00	4.5	0.0042	3.03	2.9	0.0085			
(P) pH 7.47, $\Gamma = 3.76^e$	2.07	6.9	0.0051	3.13	4.1	0.0092	3.09	4.1	0.01

^a Interatomic distance.

^b Coordination number.

^c Debye–Waller factor.

^d Zn surface coverage, $\mu\text{mol}/\text{m}^2$.

^e High-surface-area gibbsite.

In contrast, the Zn–silica spectra do not develop the split as one increased the value of R , even up to 6 Å. Therefore, noise at higher values of R do not account for the splitting phenomenon since both spectra have a similar signal to noise ratio. In the case of the Zn–gibbsite samples, the cause of the splitting could be Zn, O, or Al backscattering atoms. The same splitting feature was present in the chi spectra for Ni adsorbed as inner-sphere complexes on HSA gibbsite and was attributed to Ni–Al–Al multiple scattering paths beyond 5 Å [54]. Since multiple scattering paths were excluded in our fitting procedure, the exact nature of the splitting feature is still not known. However, given the evidence from other studies that suggests Al atoms contribute to this feature, it seems likely in our study of Zn adsorbed onto HSA gibbsite that Al multiple scattering is the likely candidate.

The structural parameters from fitting of the Zn–gibbsite EXAFS spectra are compiled in Table 4. Excluding spectra L and P, the average $R_{\text{Zn–O}} = 2.01$ Å and the average $\text{CN}_{\text{Zn–O}} = 4.8$. The average values for Zn in tetrahedral and octahedral coordination with O are 1.95 Å and 2.11 Å, respectively [15]. The average of these two values is 2.03 Å, similar to the average value obtained in our Zn–gibbsite samples, suggesting mixed coordination in our samples. In the case of spectra L, the result of 2.06 Å for Zn–O is questioned given the fact that it is the noisiest spectrum. The EXAFS signal represents the average coordination environment of all Zn atoms present in the sorption complexes and Zn has been observed to have both tetrahedral and octahedral coordination upon sorption to oxide surfaces, complexation to organic acids, and as part of the structure of minerals [18,21,55]. Therefore, it is reasonable to conclude that Zn

is present in both tetrahedral and octahedral complexes with respect to first-shell O. For the second shell, an average of $R = 3.02 \text{ \AA}$ for Zn–Al was obtained (excluding spectra L and P) and the inclusion of a Zn atom in the second shell did not improve fit quality, indicating the lack of neoprecipitate formation in these samples. Assuming $R_{\text{Al-O}} = 1.85\text{--}1.97 \text{ \AA}$ and $R_{\text{O-O}} = 2.52\text{--}2.86 \text{ \AA}$ for the gibbsite structure [56], and the average $R_{\text{Zn-O}}$ of 2.02 \AA from the sorption samples, it follows that an edge-sharing bidentate adsorption geometry (inner-sphere complex) is the main mechanism for Zn uptake on the HSA gibbsite surface. Geometric considerations would allow Zn to be in either a tetrahedral or octahedral coordination in this arrangement [57]. The $R_{\text{Zn-Al}}$ value of 3.05 \AA for sample L nearly falls in the range of values whereby an edge-sharing bidentate complex could form. The poor spectra quality as a result of low Zn concentrations makes the exact determination of Zn complexes difficult for this sample.

Comparing the Zn spectra for HSA gibbsite and LSA gibbsite (spectrum P, Fig. 5) one notes significant differences. More structural features are evident in the LSA gibbsite sample, most notably a split in the third oscillation of the chi spectrum at $k \approx 8 \text{ \AA}^{-1}$, the presence of shoulders on the oscillations in the chi spectra, and a less-dampened signal with increased k . Also, in the Fourier-transformed data one notes the appearance of a much larger second shell at slightly higher R values. Fit results indicate that Zn formed a Zn–Al LDH phase upon sorption to the LSA gibbsite. Comparison of spectrum P with the synthesized Zn–Al LDH in Fig. 3 reveals the similarity in the two spectra, which are rather distinct from other Zn-bearing minerals. The values $R_{\text{Zn-O}} = 2.07$, $R_{\text{Zn-Al}} = 3.13 \text{ \AA}$, and $R_{\text{Zn-Zn}} = 3.09 \text{ \AA}$ are similar to the Zn–O, Zn–Al, and Zn–Zn shells in synthesized Zn–Al LDH (Table 3). Similar findings have been reported for Zn adsorbed on $\alpha\text{-Al}_2\text{O}_3$ and pyrophyllite at $\Gamma > 1.7 \text{ \mu mol m}^{-2}$ and $0.8 \text{ \mu mol m}^{-2}$ Zn coverage, respectively [20,22]. These results confirm that the slow sorption of Zn on LSA gibbsite was a result of Zn–Al LDH formation, whereas the more rapid kinetics of Zn sorption on HSA gibbsite was a result of inner-sphere, bidentate Zn complex formation. Much like the Zn–silica system, aging the sample for 18 months in the presence of HSA gibbsite did not result in identifiable changes in Zn speciation.

3.5. Comparison of the silica and gibbsite sorption systems

The finding that Zn favors either octahedral (low pH) or tetrahedral (high pH) first-shell coordination when complexed to silica compared to a mixture of the two coordination environments over all pH ranges on HSA gibbsite leads one to question how the solid phase influences Zn coordination. It has previously been demonstrated for Zn that the two different coordination environments are energetically similar [58]. Moreover, the influence of reaction conditions on Zn coordination has been demonstrated in several studies, with the solid phase influencing the complex in many cases

[17,20]. In order to directly compare the two solids used in this study, it is important to select samples with similar pH values, surface loading, reaction time, and Zn concentrations in order to eliminate other variables aside from the sorbent identity. Two pairs of samples have been selected for this: low-pH samples C and J and circumneutral-pH samples H and O (Table 1). For the low-pH samples, Zn first-shell coordination environments are similar in the silica and gibbsite systems, with both samples having $R_{\text{Zn-O}}$ values (2.02 and 1.99 \AA , respectively) intermediate between typical tetrahedral and octahedral coordination. For the circumneutral samples (H and O), Zn first-shell coordination was tetrahedral in the case of silica, but remained a mixture of tetrahedral and octahedral for gibbsite. This suggests that increased pH values account for the change in coordination for Zn adsorbed on silica, but in the case of gibbsite first-shell coordination is insensitive to pH changes.

The influence of pH on metal cation adsorption onto metal oxides has been well documented and reviewed, and it is generally agreed that pH influences both the surface acidity of the functional groups on the oxides and the hydrolysis of the metal ions [4]. The difference in pH_{PZC} of the two solids (<2 for silica, 9 for gibbsite) demonstrates the difference in the acidity of the functional groups, with silica considered a strong solid acid whereas gibbsite is not [59]. Whether or not the difference in surface acidity for the two different solid phases is the reason for the differences in first-shell coordination of Zn cannot be proved from our results. We speculate that both Zn hydrolysis and surface acidity are part of the mechanism, along with other physical and chemical properties of the solid phase that are not characterized in this study. In addition, the Al atom in gibbsite may also influence the Zn complex formed, as indicated by the Zn–Al–Al multiscattering that is likely occurring in the Zn–gibbsite samples. The observation that Zn first-shell coordination environment is influenced by the solid surface demonstrates the uniqueness of Zn compared to other transition metals.

4. Summary

Zn sorption on amorphous silica and HSA gibbsite was characterized by rapid kinetics with no dependence on ionic strength. Under the studied reaction conditions, EXAFS confirmed Zn complexation via the formation of inner-sphere surface complexes as the major mechanism of adsorption for both sorbent–sorbate systems, suggesting this mechanism accounted for the observed rapid sorption kinetics. Inner-sphere complex formation on gibbsite was further confirmed by demonstrating Al backscattering paths were most likely causing the observed split in the oscillation of the first-shell of the chi data. For the LSA gibbsite, Zn–Al LDH formation became a viable sorption mechanism at pH and initial Zn concentrations similar to previous studies [22]. In the case of Zn sorption on silica, a precipitate formed at the highest pH value and resembled an amorphous $\text{Zn}(\text{OH})_2$ phase.

Based on the first-shell coordination environment around Zn obtained from EXAFS, the reaction pH and the sorbent phase may dictate the coordination environment of the adsorbed metal ion. For the Zn–silica system this is evident as Zn formed octahedral complexes with first-shell oxygen atoms in functional groups on the silica surface, changing to tetrahedral complexes with increased pH. Zn inner-sphere complexes on gibbsite were a mix of octahedral and tetrahedral with respect to first-shell O coordination, regardless of pH. This potential control of Zn coordination by the sorbent phase has important implications when it comes to complexation of metal ions in soils and sediments and, therefore, in metal ion mobility and fate.

The dynamic reactivity of Zn in the presence of important geosorbents found in soil and sediments has been demonstrated in this study. Specifically, Zn has been observed to form both tetrahedral and octahedral inner-sphere sorption complexes on oxide surfaces and precipitate as both octahedral and tetrahedral Zn hydroxide phases, depending on the reaction conditions and identity of the sorbent phase. This is in agreement with both laboratory and field-based studies that have observed Zn speciation to be extremely variable. The results of this study will be useful in order to construct reactive transport and surface complexation models capable of predicting Zn behavior in natural settings.

Acknowledgments

The authors are grateful to the staff at beamline X-11a at the National Synchrotron Light Source for assistance in EXAFS data collection. Jeffery Post (Smithsonian Institute) provided Zn reference minerals and Noriko Yamaguchi synthesized and provided the HSA gibbsite. Stefan Hunger measured Al-NMR for gibbsite. Thanks to Maarten Nachtegaal for collecting EXAFS data for zincite. This manuscript benefited from an anonymous review. D.R. Roberts appreciates the support of a National Science Foundation graduate research fellowship.

References

- [1] J.A. Coston, C.C. Fuller, J.A. Davis, *Geochim. Cosmochim. Acta* 59 (1995) 3535.
- [2] E. Baumgarten, U. Kirchhausen-Dusing, *J. Colloid Interface Sci.* 194 (1997) 1.
- [3] K.M. Spark, B.B. Johnson, J.D. Wells, *Eur. J. Soil Sci.* 46 (1995) 621.
- [4] D.G. Kinniburgh, M.L. Jackson, in: M.A. Anderson, A.J. Rubin (Eds.), *Adsorption of Inorganics at Solid–Liquid Interfaces*, Ann Arbor, Ann Arbor, MI, 1981, p. 91.
- [5] L.M. Shuman, *Soil Sci. Soc. Am. J.* 41 (1977) 703.
- [6] G. Sposito, in: J.S. Davis, K.F. Hayes (Eds.), *Geochemical Processes at Mineral Surfaces*, American Chemical Society, Washington, DC, 1986, p. 217.
- [7] S.E. Fendorf, G.M. Lamble, M.G. Stapleton, M.J. Kelley, D.L. Sparks, *Environ. Sci. Technol.* 28 (1994) 284.
- [8] R.L. Chaney, in: A.D. Robson (Ed.), *Zinc in Soils and Plants*, Kluwer Academic, Dordrecht, 1993, p. 135.
- [9] C.P. Huang, A. Rhoads, *J. Colloid Interface Sci.* 131 (1989) 289.
- [10] N.N. Vlasova, N.K. Davidenko, *Colloids Surf. A* 104 (1995) 53.
- [11] D.V. Ladonin, *Eurasian Soil Sci.* 30 (1997) 1478.
- [12] A.I. Metwally, A.S. Mashhady, A.M. Falatah, M.Z. Reda, *Pflanzen-ernähr. Boden.* 156 (1993) 131.
- [13] Y. Xu, F.W. Schwartz, S. Traina, *J. Environ. Sci. Technol.* 28 (1994) 1472.
- [14] A.M. Scheidegger, D.L. Sparks, *Soil Sci.* 161 (1996) 813.
- [15] G.A. Waychunas, C.C. Fuller, J.A. Davis, *Geochim. Cosmochim. Acta* 66 (2002) 1119.
- [16] M.L. Schlegel, A. Manceau, L. Charlet, *J. Phys. IV* 7 (1997) 823.
- [17] P. Trivedi, L. Axe, T.A. Tyson, *J. Colloid Interface Sci.* 244 (2001) 230.
- [18] L. Bochatay, P. Persson, *J. Colloid Interface Sci.* 229 (2000) 593.
- [19] T.P. Trainor, J.P. Fitts, A.S. Templeton, D. Grolimund, G.E. Brown Jr., *J. Colloid Interface Sci.* 244 (2001) 239.
- [20] T.P. Trainor, G.E. Brown Jr., G.A. Parks, *J. Colloid Interface Sci.* 231 (2000) 359.
- [21] S. Ghose, *Acta Crystallogr.* 17 (1964) 1051.
- [22] R.G. Ford, D.L. Sparks, *Environ. Sci. Technol.* 34 (2000) 2479.
- [23] M. Schlegel, A. Manceau, L. Charlet, D. Chateigner, J.-L. Hazemann, *Geochim. Cosmochim. Acta* 65 (2001) 4155.
- [24] P.A. O'Day, G.E. Brown Jr., G.A. Parks, *J. Colloid Interface Sci.* 165 (1994) 269.
- [25] A.M. Scheidegger, G.M. Lamble, D.L. Sparks, *Environ. Sci. Technol.* 30 (1996) 548.
- [26] K.G. Scheckel, A.C. Scheinost, R.G. Ford, D.L. Sparks, *Geochim. Cosmochim. Acta* 64 (2000) 2727.
- [27] A. Manceau, B. Lanson, M.L. Schlegel, J.C. Hargé, M. Musso, L. Eybert-Bérard, J.-L. Hazemann, D. Chateigner, G.M. Lamble, *Am. J. Sci.* 300 (2000) 289.
- [28] D.R. Roberts, A.C. Scheinost, D.L. Sparks, *Environ. Sci. Technol.* 36 (2002) 1742.
- [29] P.A. O'Day, S.A. Carroll, G.A. Waychunas, *Environ. Sci. Technol.* 32 (1998) 943.
- [30] M.-P. Isaure, A. Laboudigue, A. Manceau, G. Sarret, C. Tiffreau, P. Trocellier, G. Lamble, J.-L. Hazemann, D. Chateigner, *Geochim. Cosmochim. Acta* 66 (2002) 1549.
- [31] B.C. Bostick, C.M. Hansel, M.J. La Force, S. Fendorf, *Environ. Sci. Technol.* 35 (2001) 3823.
- [32] K.G. Scheckel, D.L. Sparks, *J. Colloid Interface Sci.* 229 (2000) 222.
- [33] J.H. Kyle, A.M. Posner, J.P. Quirk, *J. Soil Sci.* 26 (1975) 32.
- [34] R.M. Taylor, *Clay Miner.* 19 (1984) 591.
- [35] H.G. Dietrich, J. Johnston, *J. Am. Chem. Soc.* 49 (1927) 1419.
- [36] C.F. Baes, B.E. Mesmer, *The Hydrolysis of Cations*, Wiley, New York, 1976.
- [37] E. Libowitzky, A.J. Schultz, D.M. Young, *Z. Kristallogr.* 213 (1998) 659.
- [38] A.M. Scheidegger, D.G. Strawn, G.M. Lamble, D.L. Sparks, *Geochim. Cosmochim. Acta* 62 (1998) 2233.
- [39] D.R. Roberts, A.M. Scheidegger, D.L. Sparks, *Environ. Sci. Technol.* 33 (1999) 3749.
- [40] E.J. Elzinga, D.L. Sparks, *J. Colloid Interface Sci.* 213 (1999) 506.
- [41] P.A. O'Day, C.J. Chisholm-Brause, S.N. Towle, G.A. Parks, G.E. Brown Jr., *Geochim. Cosmochim. Acta* 60 (1996) 2515.
- [42] F.W. Lytle, R.B. Greeger, D.R. Sandstorm, E.C. Marques, J. Wong, C.L. Spiro, G.P. Huffman, F.E. Huggins, *Nucl. Instrum. Methods Phys. Res.* (1984) 542.
- [43] T. Ressler, *J. Synchrotron Rad.* 5 (1998) 118.
- [44] S.L. Zabinsky, J.J. Rehr, A. Ankudinov, R.C. Albers, M. Eller, *J. Phys. Rev. B Condens. Matter* 52 (1995) 2995.
- [45] A.M. Scheidegger, G.M. Lamble, D.L. Sparks, *J. Colloid Interface Sci.* 186 (1997) 118.
- [46] D.L. Sparks, *Environmental Soil Chemistry*, Academic Press, San Diego, 1995.
- [47] M.M. Benjamin, J.O. Leckie, *J. Colloid Interface Sci.* 79 (1981) 1999.
- [48] N. Yamaguchi, A.C. Scheinost, D.L. Sparks, *Soil Sci. Soc. Am. J.* 65 (2001) 729.

- [49] K.G. Scheckel, D.L. Sparks, *Soil Sci. Soc. Am. J.* 65 (2001) 685.
- [50] G. Wilkinson, *Comprehensive Coordination Chemistry*, Pergamon, Oxford, 1987.
- [51] S. Cheah, G.E.J. Brown Jr., G.A. Parks, *J. Colloid Interface Sci.* 208 (1998) 110.
- [52] A. Manceau, *Can. Mineral.* 28 (1990) 321.
- [53] A. Manceau, M.L. Schlegel, M. Musso, V.A. Sole, C. Gauthier, P.E. Petit, F. Trolard, *Geochim. Cosmochim. Acta* 64 (2000) 3643.
- [54] N. Yamaguchi, A.C. Scheinost, D.L. Sparks, *Clays Clay Miner.* 50 (2002) 784.
- [55] G. Sarret, A. Manceau, L. Spadini, J.-L. Hazemann, Y. Soldo, L. Eybert-Berard, J.-J. Menthonnex, *Environ. Sci. Technol.* 32 (1998) 1648.
- [56] H. Saalfeld, M. Wedde, *Z. Kristallogr.* 139 (1974) 129.
- [57] J.R. Bargar, G.E. Brown Jr., G.A. Parks, *Geochim. Cosmochim. Acta* 61 (1997) 2617.
- [58] M. Pavlov, E.M. Siegbahn, M. Sandström, *J. Phys. Chem. A* 102 (1998) 219.
- [59] C.P. Huang, Y.S. Hsieh, S.W. Park, M.O. Corapcioglu, A.R. Bowers, H.A. Elliot, in: J.W. Patterson, R. Passion (Eds.), *Metals Speciation, Separation, and Recovery*, Lewis, Chelsea, MI, 1987, p. 91.
- [60] H. Effenberger, K. Mereiter, J. Zemann, *Z. Kristallogr.* 156 (1981) 233.
- [61] K. Kihara, G. Donnay, *Can. Mineral.* 23 (1985) 647.
- [62] A.N. Christensen, *Acta Chem. Scand.* 23 (1969) 2016.
- [63] M. Bellotto, B. Rebours, O. Clause, J. Lynch, D. Bazin, E. Elkaim, *J. Phys. Chem.* 100 (1996) 8527.
- [64] R.F. Cooley, J.S. Reed, *Am. Ceram. Soc. Bull.* 50 (1972) 8.
- [65] W.S. McDonald, D.W. Cruickshank, *Z. Kristallogr.* 124 (1967) 180.
- [66] C. Hang, M.A. Simonov, N.V. Belov, *Sov. Phys. Crystallogr.* 15 (1970) 387.